Journal of Molecular Catalysis A: Chemical 304 (2009) 77–84

Contents lists available at ScienceDirect

Journal of Molecular Catalysis A: Chemical

journal homepage: www.elsevier.com/locate/molcata

A comparison between ring-opening of decalin on Ir-Pt and Ni-Mo carbide catalysts supported on zeolites

K. Chandra Mouli, V. Sundaramurthy, A.K. Dalai*

Catalysis and Chemical Reaction Engineering Laboratories, Department of Chemical Engineering, University of Saskatchewan, Saskatoon, SK S7N 5A9, Canada

ARTICLE INFO

Article history:
Received 31 July 2008
Received in revised form 15 January 2009
Accepted 18 January 2009
Available online 24 January 2009

Keywords:
HY
Hbeta
Ring-opening
Molybdenum carbide
Platinum
Iridium
Decalin

ABSTRACT

Selective ring-opening (RO) of decalin over the catalysts comprising of Pt-Ir and Ni-Mo carbide supported on HY and Hbeta was compared in a trickle bed reactor. The catalysts were synthesized by incipient wetness impregnation method and characterized by elemental analysis, BET surface area measurement, XRD, TPR and TPD of ammonia. XRD of the carbide catalysts showed no bulk molybdenum peaks and the structure did not collapse in the carburization process. TPD of ammonia showed a large amount of acidic sites on the HY-supported Pt-Ir and Ni-Mo carbide catalysts. The HY-supported Pt-Ir and Ni-Mo carbide catalysts showed higher RO activity and RO products selectivity than the corresponding Hbeta catalysts. The activity and selectivity of the Pt-Ir catalysts on H-Y are greater than Hbeta. A maximum RO yield of 33.5% was observed with the HY-supported Ni-Mo carbide catalyst. The yield and selectivity with the carbide catalysts supported on HY are comparable with that of HY-supported noble metal catalysts.

1. Introduction

Environmental concerns and regulations require severe upgrading of gas oils to get clean-burning transportation fuels. High performance diesel fuel should have high cetane number, low density and low emissions after burning. The preferable order for better quality of these parameters is paraffins, naphthenes and aromatics. The cetane number increases with ring saturation and ring-opening. The present gas oil upgrading technology employing hydrotreating in which aromatics are converted to naphthenes is not good enough because the cetane number of the naphthenes is low. Further, the high density of naphthenes gives reduced volume of the distillate fuel blend relative to a composition containing similar concentration of paraffins instead of naphthenes. Since combustion of naphthenes in fuels occurs under oxidizing conditions, there is a potential for naphthenes to reconvert to aromatics under combustion conditions, thus further reducing fuel quality. Therefore selective ring-opening (SRO) of naphthenes to paraffins is essential to upgrading the gas oil.

The currently available methods for removing the polyaromatics are (1) aromatic saturation (ASAT) and (2) hydrocracking. However, these two methods have limitations. Aromatic saturation cannot achieve the required cetane number even though it maintains the high molecular weight. Hydrocracking on the other hand increases the cetane number significantly but the molecular weight decreases greatly. So, in order to achieve the above-mentioned parameters the best alternative is selective ring-opening (SRO) of polynuclear aromatics to paraffins where cetane number is increased significantly without losing the molecular weight. Complete saturation of polynuclear aromatics to polynuclear naphthenes prior to SRO is important. Metal- and aci-site-promoted hydrocracking and dealkylation reactions must be avoided to minimize losses in middle distillate yield [1–5]. Controlling the inter conversion of six- and five-membered rings via an acid-catalyzed ring-contraction step is also of special importance, since selective conversion of six-membered naphthene rings to five-membered naphthene rings greatly influences ring-opening rates and selectivity [1,6,7].

In acid-catalyzed carbocation cleavage of ring C—C bonds, the unacceptably low yields of SRO products result from domination of the metal function by the strong acidity function where excessive side chain and product alkane cracking take place [8]. Hydrogenolysis of alkyl-substituted naphthenes can be achieved by either endocyclic or exocyclic C—C bond cleavage where the endocyclic C—C bond cleavage leads to selective ring-opening. A review on the chemistry and mechanism on selective ring-opening catalysts is available [5]. Many papers have been published in the open literature about the selective ring-opening of naphthenic compounds on noble metals supported on acidic supports [1–7,9]. However these noble metals are costly and prone to the sulfur poisoning. The alternative is carbide catalysts which show good resistance to sulfur poisoning and is also cheap. Due to their refractory nature they are resistant to sintering and attrition under reaction conditions. The

* Corresponding author. Tel.: +1 306 966 4771; fax: +1 306 966 4777.
E-mail address: ajay.dalai@usask.ca (A.K. Dalai).

1381-1169/$ – see front matter © 2009 Elsevier B.V. All rights reserved.
doi:10.1016/j.molcata.2009.01.027

objective of the present work is to study the RO reaction over metal carbide loaded on various supports such as zeolites (HY, Hbeta), mesoporous materials (Al-SBA-15), alumina and silica-alumina. In this study, decalin RO is studied under industrial conditions over Ni-promoted Mo carbide catalysts supported on the above-mentioned supports and the RO activity of most active carbide catalysts is compared with the noble metal catalysts of the same support.

2. Experimental

2.1. Catalyst preparation

The NH_4 form of HY and Hbeta (Zeolyst International) were calcined at 500 °C to be converted to the proton form. The 1.5% Pt-0.75% Ir supported on HY and Hbeta were prepared by using precursors $IrCl_3$ (Aldrich) and H_2PtCl_6 (Aldrich). The aqueous solution of iridium and platinum precursors was prepared and the supports were impregnated with the solution by the incipient wetness method. The impregnated catalysts were calcined for 3 h at 500 °C in the presence of air.

The Ni-Mo carbide (2.5 wt.% Ni and 12 wt.% Mo) catalysts supported on commercial HY, Hbeta, silica-alumina, γ-alumina and also Al-SBA-15 synthesized in our laboratory were prepared in two stages. The Al-SBA-15 synthesis and characterization are reported in our previous work [10]. In the first stage, the oxide form of the catalysts was prepared by the wet impregnation method from the precursors. The precursors for Ni and Mo are nickel nitrate (99% BDH) and ammonium heptamolybdate (99.9% Aldrich). The impregnated catalysts were dried at 120 °C for 5 h and calcined at 500 °C for 5 h. 20% CH_4/H_2 (v/v) was used to convert the oxide form catalysts into the carbide form. In the setup used to synthesize the carbide form of catalysts, the oxide form catalyst was placed at the center of an inconel reactor which is surrounded by a temperature-programmed furnace. The sample was heated from room temperature to 400 °C in the presence of He at a ramping rate of 3 °C/min. Then, the gas is switched to 20% CH_4/H_2 (v/v) and the sample was heated up to 700 °C at a ramping rate of 1 °C/min. Outlet gases from the reactor were analyzed for CO and CO_2 by using a gas chromatograph (HP 5890). The reaction was carried out until there was no formation of CO and CO_2. Then the gas was shifted to He from CH_4/H_2 and the system was cooled down to room temperature. The carbide catalysts were passivated by using 1% O_2 in He (v/v) for 4 h to avoid strong bulk oxidation. The synthesis and characterization of Ni-Mo/γ-alumina carbide catalysts are reported in our earlier paper [11].

2.2. Characterization

Plasma atomic emission method (ICP) was used for the elemental analysis of Ni, Mo, Al and Si. The carbon content of the carbide catalysts was determined by using a CHNSO analyzer (Elementar Americas Inc.). The BET surface area, pore volume, and pore size measurements of the catalysts were performed using Micrometrics adsorption equipment (Model ASAP 2000, Micrometrics Instruments Inc.) at 78 K using liquid N_2. Before analysis, the sample (0.1 g) was evacuated at 473 K for 4 h in a vacuum of 5×10^{-4} atm to remove all adsorbed moisture from the catalyst surface and pores.

Powder X-ray diffraction (XRD) patterns of the catalysts were recorded on a Bruker diffractometer using Cu Kα radiation. The CO uptake on the catalysts was measured using the Micromeritics ASAP 2000 instrument. Before chemisorption measurement, 200 mg of sample was reduced with H_2 at 400 °C, and then evacuated until the static pressure decreased to less than 6.6×10^{-4} Pa. Pulses of CO were passed over the sample to measure the total gas uptake at 35 °C.

The temperature-programmed desorption (TPD) of ammonia was performed using a Quantachrome equipment (Model Chem-BET 3000, Quantachrome Corporation) for the measurement of the total acidity of catalysts. 0.1 g sample was placed in an adsorption vessel (U-shaped) and activated at 400 °C in H_2 flow for 2 h (heating rate 10 °C/min). Then the sample was cooled to 100 °C in He flow. At this temperature, 0.1% NH_3 in N_2 was passed through the sample for 1 h followed by cooling to room temperature in He flow. TPD was carried out from room temperature to 500 °C at a heating rate of 10 °C/min with He flow at a rate of 35 ml/min. After each TPD, the amount of ammonia adsorbed was determined from the calibration curve obtained from varying volumes of ammonia in He.

Temperature-programmed reduction (TPR) analysis was performed using the Quantachrome equipment. The sample U-tube containing 0.1 g of catalyst was placed in an electric furnace and heated from 30 to 600 °C at 10 °C/min and atmospheric pressure in a reducing gas of 3 mol% H_2 in N_2 (Praxair) with a flow rate of 30 ml/min. H_2 consumption during the TPR experiments was measured with a thermal conductivity detector (TCD). The TPR plots were logged using an on-line data acquisition system.

2.3. Catalytic study

Decalin was chosen as the model reactant for the hydrogenation and ring-opening of naphthenes. The catalytic experiments were performed in a trickle bed reactor under typical industrial conditions. The high-pressure reaction setup used in this study simulates the process that takes place in an industrial hydrotreater. The system consisted of liquid and gas feeding sections, a high-pressure reactor, a heater with a temperature controller for precisely controlling the temperature of the catalyst bed and a high-pressure gas–liquid separator. The length and internal diameter of the reactor were 240 and 14 mm, respectively. For loading the catalyst, the reactor was packed from the bottom to the top in nine parts. The bottom 7 cm was first loaded with 3 mm size glass beads, 16 mesh, 46 mesh and 80 mesh silicon carbide. Then the catalyst bed approximately 10 cm long, was packed with 5 cm^3 of catalyst (2 g) and 12 cm^3 of 90 mesh silicon carbide. The top part of the catalyst bed was loaded with 80 mesh (0.8 cm), 46 mesh (0.8 cm), 16 mesh (0.8 cm) silicon carbide and finally with 3.5 mm glass beads (2.0 cm). The reaction was carried out at temperatures of 200–260 °C in H_2 at a total pressure of 5.0 MPa. Before each catalytic run, the catalyst was reduced in flowing H_2 at 400 °C for 4 h. The reactor was then brought to the reaction temperature and pressurized to 5 MPa. The liquid hourly space velocity (LHSV) and H_2 flow rate were maintained at 1.5 h^{-1} and 50 ml/min, respectively. The decalin feed was diluted with n-heptane at a volumetric ratio of 10:90. The liquid products were collected and were identified by using GC-MS and quantified by a Varian 3400 GC. The GC was equipped with a Varian CP-Sil 8 CB low bleed/MS capillary column (30 m–0.25 mm–0.25 μm) which is coated with a 5% phenyl 95% dimethylpolysiloxane low bleed phase. The same capillary column and temperature program are used for the Varian 3400 GC for the quantification purpose. The following temperature program was used for GC-MS: initial temperature 50 °C, initial temperature hold time of 5 min, heating rate of 10 °C/min, final temperature of 200 °C, final temperature hold time of 10 min and the detector temperature of 230 °C.

3. Results and discussion

3.1. Catalyst characterization

3.1.1. Characterization of Pt-Ir catalysts

The BET surface area, CO uptake and total acidity of HY, Hbeta supports and Pt-Ir catalysts supported on HY and Hbeta are shown

Table 1
Physicochemical properties of Pt-Ir catalysts.

Catalyst	SiO_2/Al_2O_3 molar ratio	%Pt (wt.%)	%Ir (wt.%)	BET surface area (m^2/g)	Pore volume (cm^3/g)	Mesopore area (m^2/g)	CO uptake (μmol CO/g)	Total acid strength (μmol NH_3/g)
HY	11.6	–	–	763	0.47	140	–	583
Hbeta	25	–	–	581	0.43	100	–	326
Pt-Ir/HY	13.3	1.5	0.75	641	0.45	120	25.8	371
Pt-Ir /Hbeta	27.5	1.5	0.75	530	0.41	90	20.3	160

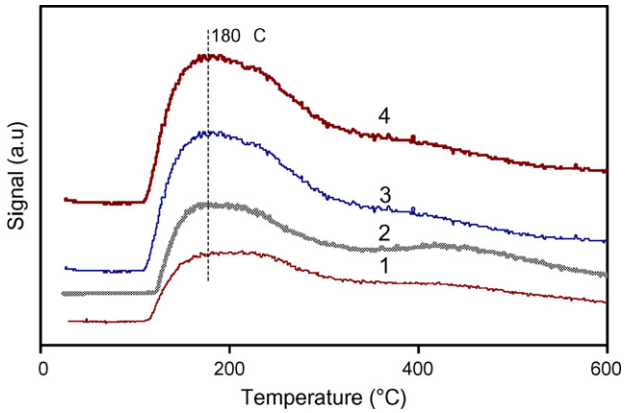

Fig. 1. NH_3–TPD graphs of (1) Pt-Ir/Hbeta, (2) Pt-Ir/HY, (3) H-beta and (4) HY catalysts.

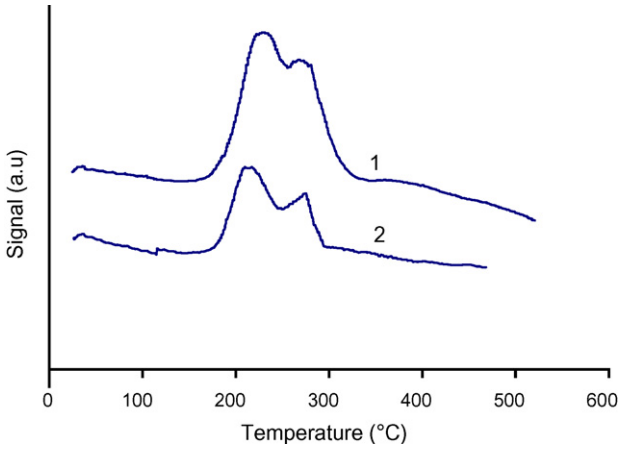

Fig. 2. TPR patterns of the (1) Pt-Ir /HY and (2) Pt-Ir/Hbeta catalysts.

in Table 1. After impregnation of supports with Ir and Pt, the surface area decreased by 10–15%. This may be due to the pore filling by the Ir and Pt. The CO uptake of the Pt-Ir catalysts is also shown in Table 1. The total acidity of the supports as well as the Pt-Ir catalysts supported on HY and Hbeta are calculated from the NH_3–TPD curves shown in Fig. 1. There is a 36–50% decrease in the total amount of acidic sites of the HY and Hbeta after impregnation. The decrease in the amount of acidic sites is due to the coverage of acid sites by the metals. From the TPD of ammonia, the acid sites are classified as weak, medium and strong [12]. In the TPD curve shown in Figs. 1 and 3, the NH_3 desorbed below 250 °C is due to weak acid sites. The NH_3 desorbed above 250 °C and below 400 °C is due to medium strength acid sites and the NH_3 desorbed above 400 °C is due to strong acid sites. In Fig. 1, the presence of a small peak between 400 and 500 °C for the Pt-Ir/HY catalyst indicated higher acid strength than the Pt-Ir/Hbeta catalyst. The TPR profiles of the Pt-Ir catalysts are displayed in Fig. 2. The Pt-Ir catalysts displayed their H_2 consumption peak at 210 to 220 °C and one more shoulder peak at 260 °C. The characteristic consumption peak at 210–220 °C with the Ir-Pt catalysts is attributed to reduction of iridium oxide [13]. The peak at 260 °C is assigned as the reduction of Pt^{2+} [14].

3.1.2. Characterization of Ni-Mo carbide catalysts

The elemental compositions, BET surface area and CO uptake of Ni-Mo carbide catalysts on HY, Hbeta, silica-alumina (Si-Al), Al-SBA-15 and γ-alumina supports are given in Table 2. Elemental chemical analysis of carbide catalysts indicates that the Mo and Ni contents are equal to or slightly less than the corresponding targeted value of 12 wt.% and 2.5 wt.%, respectively. The BET surface area of the prepared carbide catalysts is slightly lower than that of the supports. This is apparently due to pore filling of supports by the Ni and Mo species. As shown in Table 2, the Mo/C ratio of the carbide catalysts supported on HY, Si-Al, Al-SBA15 and γ-alumina is equal or slightly greater than the stoichiometric value of 2. Similar results were observed with supported carbide catalysts [15–17]. This higher Mo/C ratio indicates a strong interaction between support and molybdate [18]. Carbon monoxide was used as a molecular probe to find out the number of accessible surface metal atoms on the carbide catalysts. As shown in Table 2, the CO uptakes of carbide catalysts supported on HY and Hbeta are higher than those of other carbide catalysts. This indicates good dispersion of metal sites on the surface of the HY and Hbeta supports. CO uptake of carbide catalysts is higher than that of Pt-Ir catalysts as expected due to higher metals loading. The total acidity of all carbide catalysts is shown in Table 2 and also in Fig. 3. The carbide catalyst supported on HY shows more total acidic sites than other catalysts. The comparison of TPD profile of HY and Hbeta supports shown in Fig. 1 with those of corresponding carbide catalysts shown in Fig. 3 indicates the presence of strong acid sites in the supported metals carbide catalysts. Literature [19] showed the presence of coordinately unsaturated (CUS) Mo^{4+} sites on the surface of the support. These are well dispersed and not identified by XRD data. The strong acid sites on the carbide catalysts are may be due to these CUS sites which are Lewis acid sites. According to the acid strength definition in Section 3.1.1, the γ-alumina, silica-alumina and SBA-15 catalysts show weak acid sites, whereas the HY and Hbeta-supported carbide catalysts show medium to strong acid sites.

Table 2
Physicochemical properties of carbide catalysts.

Catalyst	Si/Al ratio	%Ni (wt.%)	%Mo (wt.%)	BET surface area (m^2/g)	CO uptake (μmol CO/g)	Total acid strength (μmol NH_3/g)	Mo/C molar ratio
NiMoC/HY	13.5	2.25	11.3	492	69	189	2.03
NiMoC/Hbeta	22.9	2.25	11.2	395	66	116	1.9
NiMoC/Al-SBA15	55.7	2.45	12	391	37	31	2.2
NiMoC/Si-Al	0.3	2.44	11.2	371	37	26	2.1
NiMoC/γ-alumina	–	2.4	11.8	199	52	27	3.2

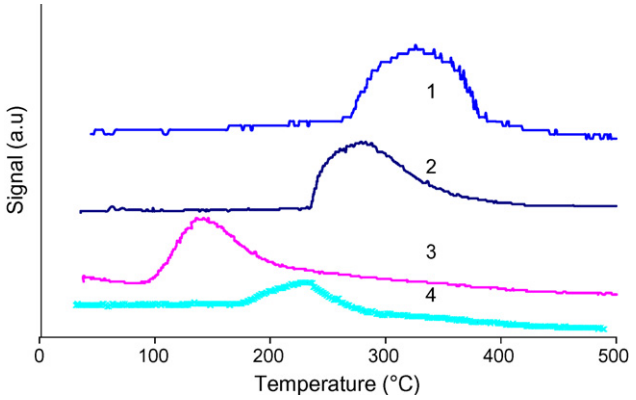

Fig. 3. NH_3–TPD plots of Ni-Mo/carbide catalysts supported on (1) HY, (2) Hbeta, (3) Al-SBA-15 and (4) silica-alumina.

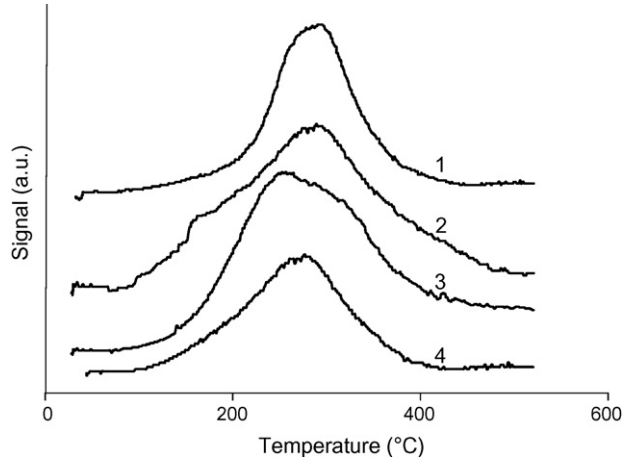

Fig. 4. TPR patterns of the passivated Ni-Mo/carbide catalysts supported on (1) HY, (2) Hbeta, (3) Al-SBA-15 and (4) silica-alumina.

H_2-TPR profiles of the passivated carbide catalysts are shown in Fig. 4. All carbide catalysts showed a major H_2 consumption peak in the range of 220–280 °C. The peaks in this range are due to the reduction of surface oxygen bonded to Mo species of different states, which were formed during the passivation of the catalysts [18]. The NiMo/γ-Al_2O_3 carbide catalyst exhibits a similar H_2 consumption peak at 255 °C, which was reported in our earlier publication [11]. The XRD patterns of HY and Hbeta supports and all carbide catalysts are shown in Fig. 5. HY and Ni-Mo carbide/HY catalysts show similar peaks in the diffractograms in agreement with the literature [20]. There is no peak representing Mo oxide or Mo carbide on the catalyst supported on HY. The characteristic peak shown by Hbeta at 2θ of 23° well matches the literature [21]. The carbide catalyst supported on Hbeta showed extra peaks at 2θ of 26° and 38° which represent Mo oxide and β-Mo_2C, respectively [22]. The crystallinity of the zeolite does not change much because the intensity of the peaks in XRD is not decreased much in the Ni-Mo carbide catalysts during the carburization process (figure not shown). The difference in the BET surface area of the carbide catalysts before and after carburization is within 3–5%, which indicates no change in the structure of the zeolite. Further more; there is no apparent evidence for molybdenum carbide in the diffractograms of the carbide catalysts supported on HY, Al-Si and Al-SBA15, which indicates good dispersion of Mo_2C-like carbides on the surface of the supports. The Mo/C ratio of different catalysts varied from 1.9 to 3.2, and in most cases close to 2, as shown by elemental and CHNSO analyses (Table 2). Therefore, we assume the formation of Mo_2C-like carbides on the surface of the catalysts. However, Mo_2C peaks could not be identified by XRD data (Fig. 5) indicating that they were well dispersed on the catalyst.

3.2. Catalytic activity

The products from the decalin ring-opening reaction are classified as follows:

(i) Cracking products (CP): Methane, ethane, propane, isobutane, isopentane, methylcyclopentane, methyl cyclohexane, n-octane, 1-octene, n-nonane, 1-nonene, 1,4-dimethylcyclohexane, propylcyclohexane, 1,3,5-trimethylcyclohexane, ethylbenzene, and ethylcyclohexane.
(ii) Ring-contraction products (RC): Methylbicyclo[4.3.0]nonane, 3,7,7-trimethylbicylco[4.1.0]heptane, 3,7-dimethylbicyclo-[3.3.0]octane, 1-methylbicyclo[3.3.1]nonane, 1,1-bicyclopentyl, spiro[4.5]decane.
(iii) Ring-opening products (RO): Butylbenzene, pentenylcyclopentane, butenylcyclohexane, 4-methyl-1-(1-methylethyl)-cyclohexene, 1-methyl-4-(1-methylethylidene) cyclohexane, 1-decene, pentylcyclopentane, butylcyclohexane, n-decane, 3,4,5-trimethylheptane, 3,5-dimethyloctane, 4-methylnonane, 3-ethyl-2-methyl heptane, and 4-ethyl-3-methyl heptane.
(iv) Dehydrogenation products (DH): Benzene, toluene, m-xylene, naphthalene, 1-methylindan, and tetralin.

The possible reaction scheme for decalin ring-opening reaction is shown in Fig. 6. The metallic sites are responsible for hydrogenation and dehydrogenation reactions whereas the Brønsted acid sites are responsible for cracking and ring-opening reactions [6,7,9]. The

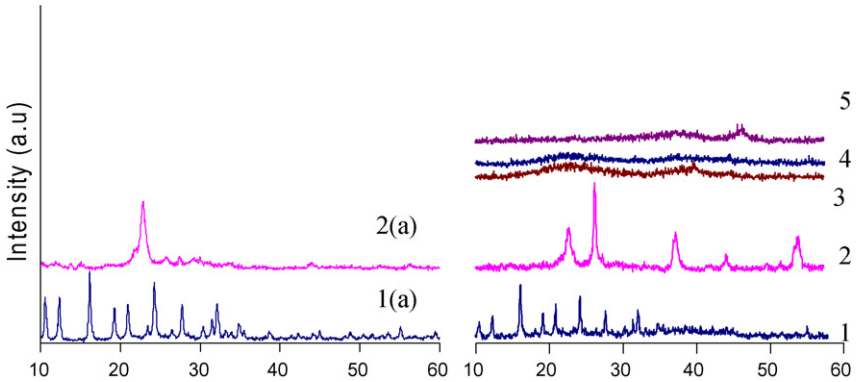

Fig. 5. XRD patterns of the Ni-Mo carbide catalysts on various supports, (1) HY, (2) Hbeta, (3) Al-SBA -15, (4) silica-alumina and (5) γ-alumina and on pure supports, (1a) HY and (2a) Hbeta.

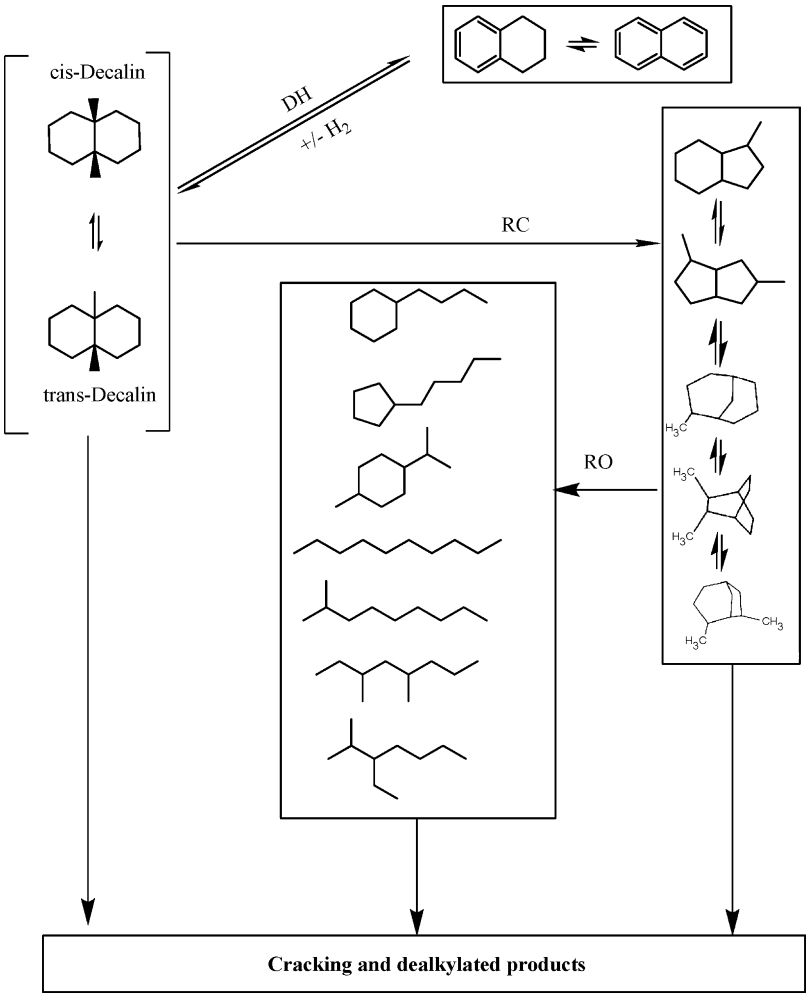

Fig. 6. Reaction scheme of decalin ring-opening reaction.

possible path toward the ring-opening products is through RC products as shown in Fig. 6. These products have been identified by GC-MS analysis of decalin ring-opening reaction. The β-scission on the ring due to endocyclic cracking leads to RO products, whereas exocyclic cracking leads to dealkylation products. Secondary cracking of the RO products results in formation of the low molecular weight cracking products.

3.2.1. Ir-Pt catalysts supported on H-Y and H-beta

The effect of temperature on the conversion of decalin on Pt-Ir supported on HY and Hbeta is shown in Fig. 7. The conversion of decalin was higher at all temperatures on the H-Y catalyst than on the Hbeta catalyst and reached almost 99% at 260 °C, as shown in Fig. 7 and Table 3. The effect of temperature on the yields of CP, RC, and DH products are given in Fig. 8. At 200 °C the yield of RC products on Pt-Ir/HY is 10%, increased to 18% at 220 °C, and then decreases. In the case of Pt-Ir/Hbeta, the RC products increased with temperature up to 260 °C and then started converting to RO products. On Pt-Ir/HY, the yield of dehydrogenation products increased with an increase in temperature from 200 to 240 °C and then decreased with increasing temperature up to 260 °C possibly due to their conversion toward coke-forming precursors. The Pt-Ir/Hbeta catalyst gave a maximum of DH products yield of 10% at 260 °C and then converted to coke-forming precursors above 260 °C. The effects of temperature on the yield and selectivity of total ring-opening products are shown in Fig. 9. The RO selectivity can be defined as the ratio of the wt.% of the RO products to the wt.% of the (RC + CP + DH) products. A maximum RO yield of 35% was obtained at 220 °C on Pt-Ir/HY, whereas Pt-Ir/Hbeta gave a maximum yield of 15% only at 260 °C. The Pt-Ir/HY catalysts show higher RO selectivity up to 220 °C compared to the Pt-Ir/Hbeta catalysts. A RO selectivity of 63% was achieved by the Pt-Ir/HY catalyst at 220 °C at which the RO yield was maximum, whereas the Hbeta-

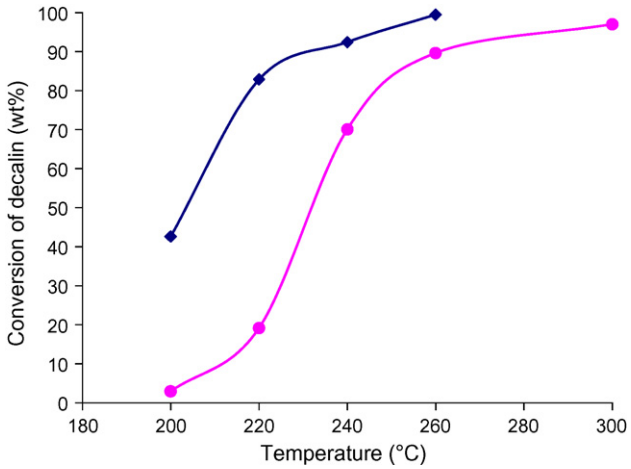

Fig. 7. Conversions of decalin on catalyst (♦) Pt-Ir/HY and (●) Pt-Ir/Hbeta as a function of temperature at a pressure of 5 MPa and LHSV of 1.5 h^{-1}.

Table 3
Comparison of RO yield and selectivity on Pt-Ir and Ni-Mo carbide catalysts supported on HY.

Catalyst	Conversion (wt.%)			RO yield (wt.%)			RO selectivity (%)		
	220 °C	240 °C	260 °C	220 °C	240 °C	260 °C	220 °C	240 °C	260 °C
Pt-Ir/HY	82.87	92.4	99.45	31.7	11.7	0.32	65.1	14.9	0.3
Ni-Mo/HYcarbide	44.3	84.6	99.8	16	33.7	16	36.2	39.8	16.3

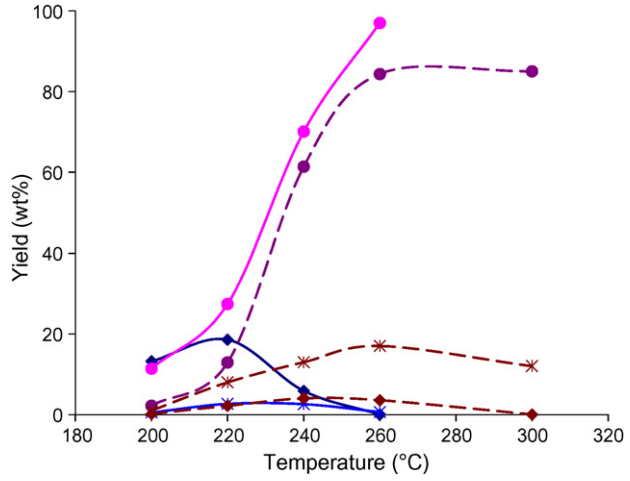

Fig. 8. The yield of cracking (●), RC (♦) and DH (×) products as a function of temperature on catalysts Pt-Ir/H-Y (solid line) and Pt-Ir/Hbeta (dotted line). (Pressure of 5 MPa and LHSV of 1.5 h^{-1}.)

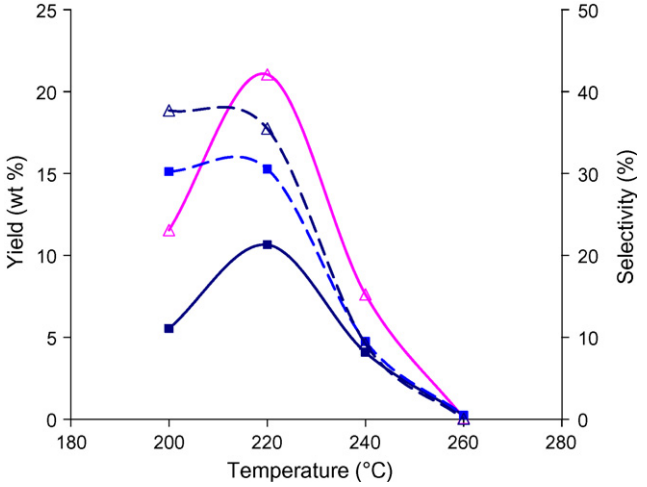

Fig. 10. The saturated and unsaturated RO yield (solid line) and selectivity (dotted line) as a function of temperature on catalyst Pt-Ir/HY at a pressure of 5 MPa and LHSV of 1.5 h^{-1}. (Saturated RO products (■); Unsaturated RO products (△).)

supported catalyst showed 12% RO selectivity at 260 °C, at which the RO yield was maximum. The effect of temperature on the yield and selectivity of saturated and unsaturated ring-opening products on Pt-Ir/HY is shown in Fig. 10. They followed the same trend as that of total ring-opening products. The yield of unsaturated products increased with increasing temperature up to 220 °C because cracking (without hydrogenation) and dehydrogenation are favored with an increase in temperature. Above 220 °C, ring-opening products underwent further cracking to form C_1 to C_6 hydrocarbons. The subtle difference between the depletion of saturated and unsaturated ring-opening products can be used to think of ways to improve their yield. The conversion of decalin does not present a problem (Fig. 7) for achieving higher RO yields but the excessive cracking eventually reduces the yield and selectivity of ring-opening products (Fig. 9).

If we reduce the yield of cracking products by decreasing the acidity of the catalyst, reaction at high temperatures may favor better ring-opening products yields. However, high temperatures favor the formation of dehydrogenation products [23] which might lead to coke-forming precursors.

Further, the opening of second ring in decalin is an important step in the view of cetane improvement. The effect of temperature on the yield and selectivity of two-ring-opening (TRO) products on Pt-Ir/HY is shown in Fig. 11. A maximum TRO selectivity of 5% at the yield of 4% was observed at 220 °C. The increase in the yield and selectivity from 200 to 220 °C is explained as follows. The yield of saturated two-ring-opening products decreases with an increase in temperature. In contrast, the yield of unsaturated two-ring-opening products increases thus making the yield and selectivity increase

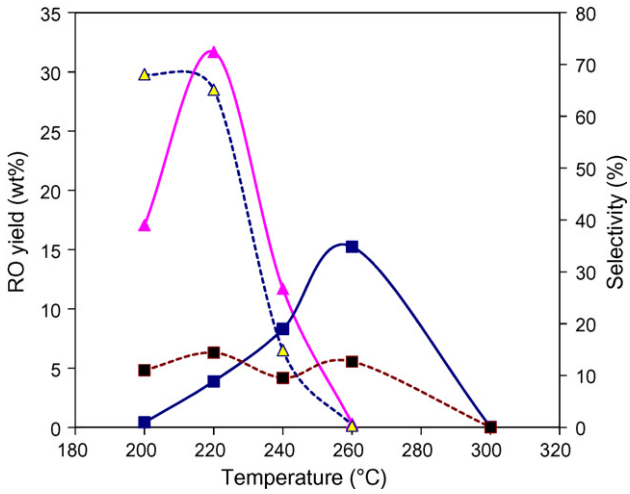

Fig. 9. The RO yield (solid line) and selectivity (dotted line) as a function of temperature on catalysts at a pressure of 5 MPa and LHSV of 1.5 h^{-1} (Pt-Ir/HY (▲); Pt-Ir/Hbeta (■)).

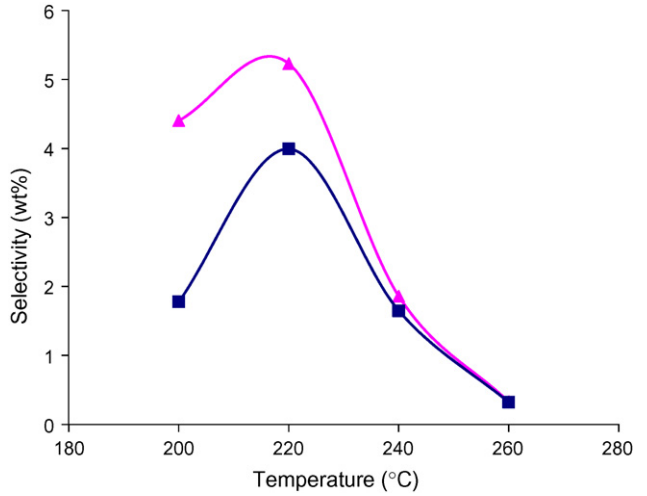

Fig. 11. The yield (■) and selectivity (▲) of two-ring-opening (TRO) products as a function of temperature on catalyst Pt-Ir/H-Y at a pressure of 5 MPa and LHSV of 1.5 h^{-1}.

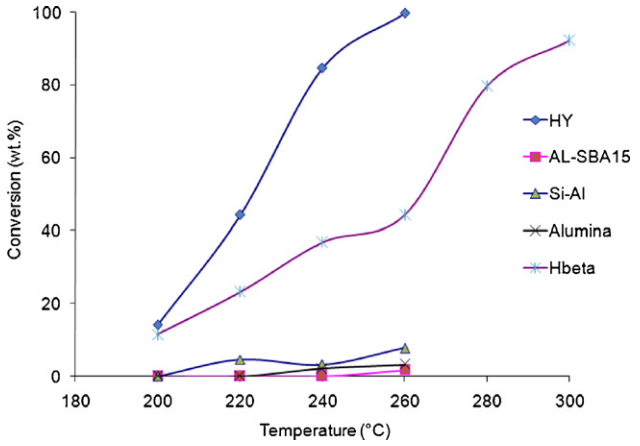

Fig. 12. The conversions of decalin as a function of temperature on Ni-Mo/carbide catalysts. Pressure = 5 MPa and LHSV = 1.5 h^{-1}.

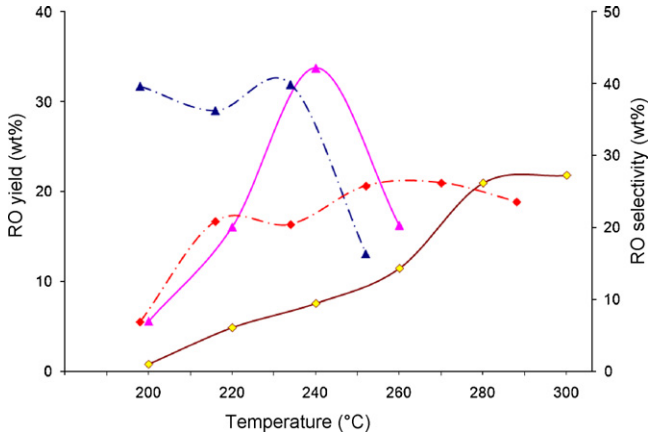

Fig. 14. The RO product yield (solid line) and selectivity (dotted line) of decalin as a function of temperature on Ni-Mo/Carbide catalysts supported on HY (▲) and Hbeta (♦). (Pressure of 5 MPa and LHSV of 1.5 h^{-1}.)

with temperature. The yields of unsaturated species such as 2,6-dimethyl-2-octene, 3-methyl-4-nonene increase with increase in temperature and beyond this temperature range excessive cracking causes the yield and selectivity to decrease. The ratio of two-ring-opening products to total ring-opening products increases with an increase in temperature which is observed in the present work and also reported in our earlier work [23].

3.2.2. Ni-Mo carbide catalysts

The conversion of decalin on Ni-Mo carbide supported on HY, Hbeta, Al-SBA-15, silica-alumina and γ-alumina is shown in Fig. 12. It was observed that the carbide catalysts supported on HY and Hbeta gave higher conversions (more than 80%), whereas carbides supported on other supports (SBA-15, silica-alumina and γ-alumina) showed negligible conversion. This is due to the weak acidity of latter sets of catalysts as evidenced by the NH_3–TPD. The Ni-Mo carbide catalysts supported on HY and Hbeta were chosen for optimization of process variables. Low temperatures (240–260 °C) favored higher conversion for the HY-supported carbide catalysts, whereas high temperatures (280–300 °C) favored higher conversion for the Hbeta-supported carbide catalysts. The deactivation behavior was observed continuously for 150 h. The conversions at different times at temperature of 260 °C are shown in Fig. 13. There was a 2% decrease in the conversion of decalin at the end of 150 h, which indicates the activity did not change much with the time

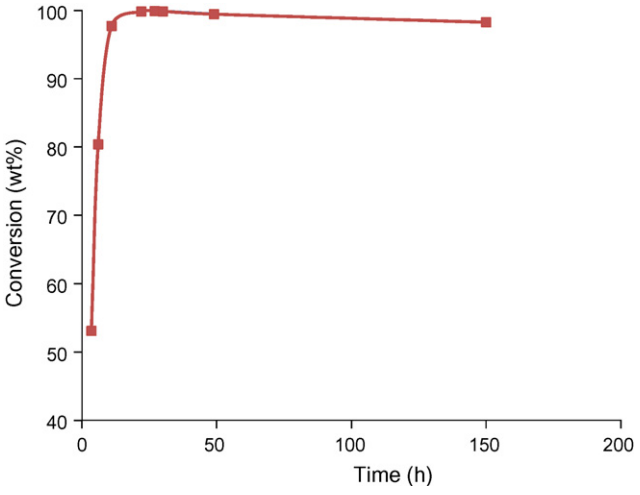

Fig. 13. Conversion of decalin on Ni-Mo carbide/HY catalysts over time on stream at a temperature of 260 °C, pressure of 5 MPa and LHSV of 1.5 h^{-1}.

period of 150 h. The products from decalin RO reaction are classified as RO, CP, RC and dehydrogenation products as discussed in Section 3.2. The ring-opening products yield with temperature on Ni-Mo carbides supported on HY and Hbeta is shown in Fig. 14. A maximum ring-opening products yield of 33.7% was observed with the HY-supported carbide catalyst at 240 °C whereas the Hbeta-supported catalyst gave a maximum of 21.8% RO yield at 300 °C. The RO selectivity on both HY and Hbeta supports are also shown in Fig. 14. A maximum of 26% selectivity was observed on Ni-Mo carbide supported on Hbeta at 280 °C, whereas Ni-Mo carbide supported on HY showed a maximum selectivity of 40% at 240 °C. Observation of the products of decalin ring-opening reaction at 200 °C on Ni-Mo carbide/HY and Ni-Mo carbide/Hbeta clearly indicates the effect of pore size on the product distribution. Even though the conversion is the same at this temperature on both the catalysts, HY gave higher yield and selectivity of ring-opening products. Due to large pore size, high mesoporous surface area and more amount of acid sites as shown in Table 2, Ni-Mo carbide supported on HY gave higher yield and selectivity of ring-opening products.

RC and cracking product yields with change in temperature on the Ni-Mo/carbide catalysts supported on HY and Hbeta are shown in Fig. 15. The RC products yield on the carbide/HY and

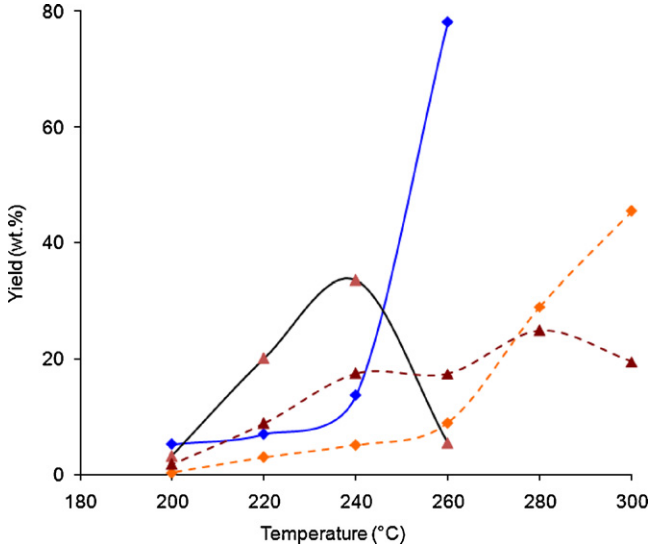

Fig. 15. The yield (wt.%) of RC (▲) and CP (♦) products as a function of temperature on Ni-Mo/carbide catalysts supported on HY (solid lines) and Hbeta (dotted lines). (Pressure of 5 MPa and LHSV of 1.5 h^{-1}.)

carbide/Hbeta catalysts shows similar trends to that observed in the previous section with noble metals. The trends clearly show that the RC products are the intermediates before converting to ring-opening products. On the HY-supported carbide catalyst the cracking is dominant above 240 °C and behaved in the same way as that of Pt-Ir/HY. But in the case of Hbeta-supported carbide catalysts, high cracking activity emerged above 260 °C. The cracking activity of Hbeta is low between 240 and 260 °C due to its low acidity, low mesopore area and small pore volume compared to HY as shown in Table 2; no access to high molecular weight molecules inside the pores is allowed. The RO yield and selectivity are compared for both Pt-Ir and Ni-Mo carbide catalysts supported on HY as shown in Table 3. At 220 °C, the maximum RO yield and selectivity are observed over the noble metal catalyst. The comparable RO yield with good RO selectivity is observed at 240 °C over the carbide catalyst. This should indicate that the Ni-Mo carbide catalyst could be an alternative to noble metal catalysts for the RO reaction.

4. Conclusions

The Ni-Mo carbide supported on HY, Hbeta, silica-alumina, γ-alumina and Al-SBA-15 catalysts were prepared for ring-opening reaction and the activity of the above catalysts are compared with noble metal catalysts. XRD patterns of the Ni-Mo carbide catalyst supported on Hbeta show the presence of β-Mo_2C, whereas with all other carbide catalysts, there is no β-Mo_2C peak in the diffractogram due to higher dispersion. CO chemisorptions show good dispersion of the metal on the support and that the available metal sites are large in number with the carbide catalysts. The total amount of acidic sites is higher for the noble metal catalysts and the acidity reduced to 30–35% for the carbide catalysts. Selective ring-opening of decalin over Ni-Mo carbide catalysts showed HY- and Hbeta-supported catalysts are the best among the carbide catalysts. These HY- and Hbeta-supported carbide catalysts were compared with the noble metals catalysts loaded on the same supports. The Ni-Mo carbide supported on HY showed a maximum yield of 33.5% at 240 °C. The Pt-Ir/HY catalyst showed a 32% RO yield at 220 °C. The saturated and unsaturated ring-opening products yields follow the same trend as the total ring-opening products yield. It was observed that the Ni-Mo carbide catalyst can be successfully used to obtain the same level of ring-opening products yield that can be achievable with noble metals catalysts.

Acknowledgement

The authors are grateful to National Center for Upgrading Technology, Devon, Alberta for their financial assistance.

References

[1] D. Kubicka, N. Kumar, P. Maki-Arvela, M. Tiitta, V. Niemi, H. Karhu, T. Salm, D.Y. Murzin, J. Catal. 222 (2004) 65.
[2] U. Nylen, B. Pawelec, M. Boutonnet, J.L.G. Fierro, Appl. Catal. A 299 (2006)14.
[3] M.A. Arribas, A. Martĩnez, Appl. Catal. A: Gen. 230 (2002) 203.
[4] M.A. Arribas, P. Concepción, A. Martĩnez, Appl. Catal. A: Gen. 267 (2004) 111.
[5] H. Du, C. Fairbridge, H. Yang, Z. Ring, Appl. Catal. A: Gen. 294 (2005) 1.
[6] D. Kubicka, N. Kumar, P. Maki-Arvela, M. Tiitta, V. Niemi, H. Karhu, T. Salm, D.Y. Murzin, J. Catal. 227 (2004) 313.
[7] M. Santikunaporn, J.E. Herrena, S. Jongpatiwut, D.E. Resasco, W.E. Alwarez, E. Sughrue, J. Catal. 228 (2004) 100.
[8] J. Weitkamp, Stefan Ernst, Catal. Today 19 (1994) 107.
[9] M. Vicker, M. daage, G.B. Touvelle, M.S. Hudson, D.P. Klein, W.C. Baird Jr., B.R. Cook, J.G. Chen, S. Hantzer, D.E.W. Vaughan, E.S. Ellis, O.C. Feeley, J. Catal. 210 (2002) 137.
[10] V. Sundaramurthy, I. Eswaramoorthi, A.K. Dalai, J. Adjaye, Microporous Mesoporous Mater. 111 (2008) 560.
[11] V. Sundaramurthy, A.K. Dalai, J. Adjaye, Catal. Today 125 (2007) 239.
[12] A. BorCave, A. Auroux, C. Guimon, Microporous Mater. 11 (1997) 275.
[13] U. Nylén, J.F. Delgado, S. Järås, M. Boutonnet, Appl. Catal. A: Gen. 262 (2004) 189.
[14] C.M.N. Yoshioka, T. Garetto, D. Cardoso, Catal. Today 107–108 (2005) 693.
[15] P.D. Costa, C. Potvin, J.M. Manoli, B. Genin, G.D. Mariadassou, Fuel 83 (2004) 1717.
[16] B. Dhandapani, S. Ramanathan, C.C. Yu, B. Fruhberger, J.G. Chen, S.T. Oyama, J. Catal. 176 (1998) 61.
[17] P.D. Costa, C. Potvin, J.M. Manoli, M. Breysse, G. Djega-Mariadassou, Catal. Lett. 72 (2001) 91.
[18] Z. Wei, Q. Xin, P. Grange, B. Delmon, J. Catal. 168 (1997) 176.
[19] B. Diaz, S.J. Sawhill, D.H. Bale, R. Main, D.C. Phillips, S. Korlann, R. Self, M.E. Bussell, Catal. Today 86 (2003) 191.
[20] A.M.G. Pedrosa, M.J.B. Souza, D.M.A. Melo, A.S. Araujo, Mater. Res. Bull. 41 (2006) 1105–1111.
[21] X. Li, W. Zhang, S. Liu, L. Xu, X. Han, X. Bao, J. Catal. 250 (2007) 55.
[22] S.J. Ardakani, X. Liu, K.J. Smith, Appl. Catal. A: Gen. 324 (2007) 9–19.
[23] K.C. Mouli, V. Sundaramurthy, A.K. Dalai, Z. Ring, Appl. Catal. A: Gen. 321 (2007) 17.